Available online at www.sciencedirect.com
ScienceDirect
Journal of Magnetic Resonance 185 (2007) 118–129
JMR Journal of Magnetic Resonance
www.elsevier.com/locate/jmr

Spin pair geometry revealed by high-field DEER in the presence of conformational distributions

Ye. Polyhach [a,b], A. Godt [c], C. Bauer [a], G. Jeschke [a,b,*]

[a] Max Planck Institute for Polymer Research, Postfach 3148, 55021 Mainz, Germany
[b] University of Konstanz, Department of Chemistry, 78457 Konstanz, Germany
[c] Bielefeld University, Department uf Chemistry, Universitätsstraße 25, 33615 Bielefeld, Germany

Received 11 September 2006
Available online 21 December 2006

Abstract

Orientation selection on two nitroxide-labelled shape-persistent molecules is demonstrated by high-field pulsed electron–electron double resonance experiments at a frequency of 95 GHz with a commercial spectrometer. The experiments are performed with fixed observer and pump frequencies by variation of the magnetic field, so that the variation of both the dipolar frequencies and the modulation depths can be analyzed. By applying the deadtime-free four-pulse double electron–electron resonance (DEER) sequence, the lineshapes of the dipolar spectra are obtained. In the investigated linear biradical and equilateral triradical the nitroxide labels undergo restricted dynamics, so that their relative orientations are not fixed, but are correlated to some extent. In this situation, the general dependence of the dipolar spectra on the observer field can be satisfyingly modelled by simple geometrical models that involve only one rotational degree of freedom for the biradical and two rotational degrees of freedom for the triradical. A somewhat better agreement of the dipolar lineshapes for the biradical is obtained by simulations based on a molecular dynamics trajectory. For the triradical, small but significant deviations of the lineshape are observed with both models, indicating that the technique can reveal deficiencies in modelling of the conformational ensemble of a macromolecule.

Keywords: EPR; ELDOR; Spin labeling; High-field EPR; Orientation selection

1. Introduction

Magnetic resonance spectroscopy is one of only a few techniques that can reveal detailed structural information on matter that lacks long-range order. As many new materials and all functional biological systems belong to this class of samples, development of new approaches for such structure elucidation is an important and constantly evolving field. In particular, pulsed electron paramagnetic resonance [1] combined with site-directed spin labeling [2–8] is recently finding more and more applications in studies of structure and functionality of synthetic and biomacromolecules, as it nicely complements NMR and scattering techniques with respect to the distance range and requirements on the sample. Distances and distance distributions between fragments of the macromolecule carrying electron spins (nitroxide spin labels, transition metal ion etc.) can be studied with high precision applying double electron–electron resonance (DEER) [9–11] or double-quantum EPR experiments [12–14] if the distance between the spins falls within the 1.5–8 nm range. Application examples of DEER include soluble [15–18] and membrane [19–22] proteins, ribonucleic acids [23], and peptides [24] as well as nanostructured materials [25–28], most of them spin-labeled.

Since the first steps made in early 1980s [9,10] a fundamental theory of that method and sophisticated data analysis approaches have been elaborated [29–36]. By now it is well understood how to select the pulse sequence and timing, the spin pair concentration, the type of the matrix, and

* Corresponding author. Fax: +49 7531 88 3139.
E-mail address: Gunnar.Jeschke@uni-konstanz.de (G. Jeschke).

1090-7807/$ - see front matter © 2006 Elsevier Inc. All rights reserved.
doi:10.1016/j.jmr.2006.11.012

the data analysis procedures to obtain structural information with the highest possible accuracy and reliability. These issues will be discussed in a forthcoming paper.

In the present work we consider the opportunities for obtaining geometric information on the structure of macromolecules beyond the distance distribution by making use of orientation selection [37,38]—an approach which is strongly aided by performing the DEER experiments at high field [39]. We examine conditions under which such experiments can best be performed with commercial spectrometer hardware. To be applicable to spin-labeled macromolecules, which are almost invariably characterized by a conformational distribution of the nitroxide labels, the approach has to accommodate distributions of the geometric parameters. The modeling of such distributions and their use in the computation of orientation-selected DEER spectra is also discussed.

The paper is organized as follows. A detailed Materials and methods section introduces the model systems, on which the measurements were performed, the set-up of the DEER experiments at high field and the measurement strategy, as well as the basic procedures for structural modeling. The subsequent Theory section starts with a description for the case of an isolated spin pair with a fixed geometrical arrangement and proceeds with the introduction of an averaging procedure that can predict the DEER response for fully geometrically uncorrelated as well as correlated spin pairs and intermediate cases. The Theory section concludes with the presentation of an computationally efficient DEER simulation approach that provides two-dimensional spectra with a dipolar frequency and a magnetic field dimension that are averaged over the distribution of relative geometries of the two paramagnetic centers. Experimental results are presented and compared with theoretical predictions in the Results and Discussions section, and the paper concludes with considerations on the applicability of the approach to spin-labeled biomacromolecules.

2. Materials and methods

2.1. Sample preparation

Two model systems with restricted conformational flexibility were used—a shape-persistent nitroxide spin-labeled biradical and a triradical (Fig. 1). Synthesis of the compounds is described in detail elsewhere [40]. Samples were prepared by dissolving approximately 0.1 mg of each compound in 100 mg of perdeuterated *o*-terphenyl. The deuterated matrix was used to increase the phase memory time T_m of the radicals [33]. Thus longer experimental dipolar evolution times can be achieved, and better dipolar frequency resolution is obtained. The crystallized mixtures were powdered in an agate mortar, placed in home-made EPR tubes (CFQ-quartz, Wilmad) with outer and inner diameters of 0.87 and 0.7 mm, respectively, and remolten with a heat gun adjusted to 100 °C air temperature. The samples were immediately placed into the EPR probehead

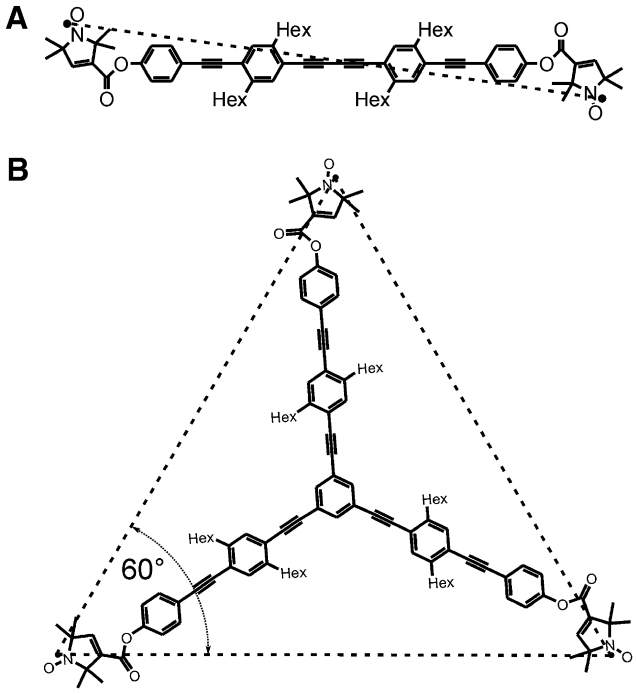

Fig. 1. Model compounds used in the orientation selection experiments. Shape persistent biradical (A) with interspin distance r_{AB} of 3.62–3.88 nm, and a shape persistent triradical (B) with r_{AB} of 2.42–4.22 nm (global maximum at 3.64–3.66 nm).

that was pre-cooled to 80 K using liquid nitrogen cooling to obtain glassy frozen solutions. Visual examination of the remolten samples revealed that they did not crystallize for several minutes at ambient conditions.

2.2. Instrumentation

DEER measurements were performed at *W*-band frequencies of approximately 94.2 GHz on the commercially available power upgraded Bruker Elexsys 680 spectrometer. The *X*-band intermediate frequency microwave (m.w.) bridge of the spectrometer was customized to allow double frequency operation by disconnecting the input m.w. from the Gunn diode of the spectrometer from the two channels of one m.w. pulse forming unit (MPFU) and replacing it by m.w. input from a HP 8350B Sweep Oscillator (2.0–18.6 GHz). The 35 mW output of the HP 8350B pump source was amplified by a AMF-5B-080120-30-25B amplifier (Miteq) to 150 mW, so that m.w. power of the observer and pump channels was the same. A Racal broadband frequency counter (10–20 GHz) was used for precise control of the pump frequency. This setup is expected to provide similar performance for DEER experiments as the commercial electron–electron double resonance (ELDOR) unit of the Bruker spectrometer. All experiments reported here were performed using a standard Bruker TeraFlex *W*-band resonator. Subsequent measurements revealed, however, better tuning conditions, better long-time stability and better reproducibility when using a newer

Bruker EN 660–1021 H *W*-Band Pulse EPR/ENDOR resonator together with sample tubes of 0.9 mm outer diameter and 0.5 mm inner diameter (Bruker). The latter probehead and sample tubes are advisable for measurements on spin-labeled proteins.

2.3. Pulse sequence, setup, and measurement strategy

All experiments were performed using the four-pulse DEER sequence $\pi/2(\nu_1) - \tau_1 - \pi(\nu_1) - \tau_0 - \pi(\nu_2) - (\tau_1 + \tau_2 - \tau_0) - \pi(\nu_1) - \tau_2 -$ echo (Fig. 2) [11]. In contrast to *X*-band frequencies where avoidance of overlap of the excitation bands of the observer pulses at frequency ν_1 and the pump pulse at frequency ν_2 is the only crucial requirement for frequency and pulse length selection, for orientation selection experiments the excitation bandwidths also have to be significantly smaller than the total width of the EPR spectrum of at least one of the coupled radicals. However, the main limitation in adjusting the pulse lengths, the frequency separation, and the placement of the m.w. frequencies with respect to the m.w. mode were imposed by the hardware. The tuning picture of the critically coupled resonator is shown on Fig. 3 (dotted line) together with a typical experimental nitroxide spectrum (solid line) and a simulated nitroxide spectrum (dashed line). The shortest possible length of the π pulse was determined by nutation experiments at full m.w. power [1] and was found to be 70–72 ns at the very center of the m.w. mode for both observer and pump source. The reliably reproducible π pulse length for that condition was 80 ns corresponding to an excitation bandwidth of approximately 15 MHz neglecting bandwidth reduction by the shape of the resonator mode. This reduction due to a lesser B_1 field enhancement in the wings of the mode was probed by observing the nutation frequency as a function of the difference between the spectrometer frequency and the center of the mode. In a range of $\pm$10–12 MHz around the center a π pulse length of 80–88 ns could be achieved for a significant fraction of spins. However, a decrease in the echo intensity accompanying the off-center shift indicates that the properly inverted spins have frequencies close to the center of the mode. To maintain sufficient pump efficiency, the pump pulse length and position were thus set to 80–88 ns and $\pm$2 MHz about the m.w. mode center, respectively. To maximize observer echo intensity and thus obtain the highest possible signal-to-noise (*s*/*n*) ratio, the length of the observer pulses was also chosen between 80 and 88 ns.

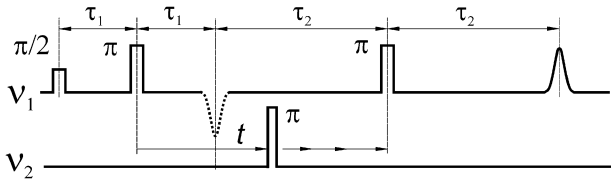

Fig. 2. Four-pulse DEER sequence. ν_1-internal spectrometer frequency; ν_2-pump frequency fed from an external HP 8350B Sweep Oscillator.

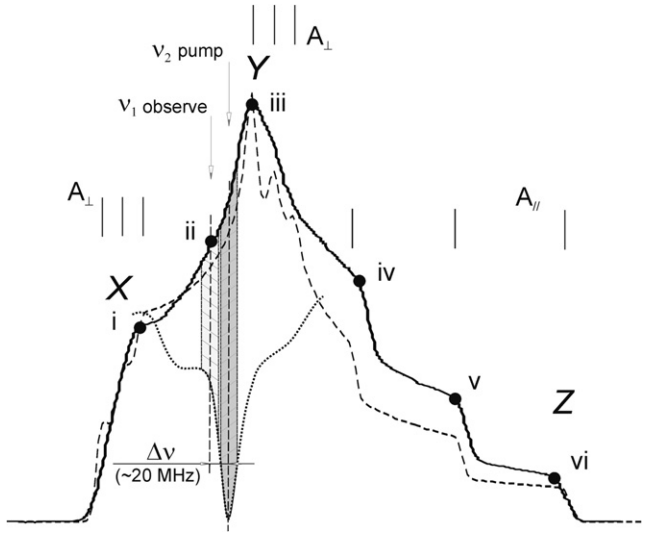

Fig. 3. Example for the setup of observer frequency ν_1 and pump frequency ν_2 with respect to the experimental echo-detected *W*-band nitroxide spectrum (solid line) and a simulated spectrum (dashed line) and to the microwave mode of a critically coupled Bruker TeraFlex *W*-band resonator (dotted line). Shaded areas indicate excitation bands. The full circles denoted with i, ii, iii etc. indicate experimental sampling positions. Simulation parameters: $g_{xx} = 2.0090$, $g_{yy} = 2.0060$, $g_{zz} = 2.0024$, and $A_\perp = 6.5$ G, $A_{//} = 34.3$ G.

The same length was used for all observer pulses to keep excitation bandwidth in the observer sequence constant and avoid unwanted excitation of pumped spins by observer pulses.

For selecting the observer position we considered the excitation profile of the three-pulse refocused echo subsequence, which is close to Gaussian with no sidebands [11,34]. For the pump pulse, sidebands are present [34], but are somewhat attenuated at the observer position in the wing of the m.w. mode when the pump position is in a 2 MHz vicinity of the m.w. mode center and the separation to the observer position is at least 15 MHz. This value can be considered as a lowest safe limit at which observer and pump frequencies do not overlap when 80 ns π-pulses are applied. In all reported measurements, the pulse length of all pulses (observer and pump) was set to 80 ns, and a 20 MHz pulse separation was applied. For our model systems the excitation bandwidth is thus still much larger than the dipole–dipole coupling between the two electron spins.

The dipolar evolution time *t* (Fig. 2) was chosen to be 4 and 2.5 μs for biradical and triradical, respectively, providing a good resolution in dipolar frequency domain, since at least two complete dipolar oscillations could be observed in the time domain for $t_d = 2.5$ μs. The separation τ_1 of the observer $\pi/2$ and π pulses was set to 300 ns.

For setup of the orientation selection experiment, we first acquired an electron spin echo detected EPR spectrum (ESE spectrum) (Fig. 3). A set of the magnetic field positions for DEER measurements was then selected, and the external magnetic field B_0 was set to one of them, usually first to the global maximum of the spectrum (position iii

on Fig. 3). Then the pump pulse was adjusted with coinciding observer and pump frequencies close to the center of the mode, using an echo inversion sequence with the inversion pulse from the pump source and the two other pulses from the spectrometer source. After that, the pump frequency was kept fixed, the spectrometer frequency was shifted by 20 MHz (the pulse separation) and the observer pulses were adjusted. All subsequent DEER measurements at different sampling positions in the spectrum were performed without changing either pump or observer frequency or any pulse parameters. This methodology assures that modulation depths can be meaningfully compared and used in data analysis. It is different from the one applied in [39] where the pump frequency was fixed and the orientation selection was done by varying the observer frequency. In our methodology, the pump and the observer frequencies are set very close to each other, which allows for critical resonator coupling and thus efficient use of limited pulse power. Furthermore, very close orientations of the pump and observer spins are experimentally selected, which aids intuitive understanding of the results.

Measurement time of the DEER experiments was selected to ensure a reasonable signal-to-noise (s/n) ratio at all sampling positions and was thus varied with sample position. The shortest typical measurement time was 2–3 h when measuring in the vicinity of Y orientations of the nitroxide g-tensor. Achieving comparable s/n ratios when sampling Z orientations of the g-tensor required much longer measurement times of up to 40–50 h. To avoid drifts of the m.w. mode during measurements, the spectrometer and probehead had to be thermally equilibrated for up to 2–3 h.

2.4. Structural models for the biradical and triradical

Two structure models were tested, which are referred to as the *simple geometrical model* and the *molecular dynamics (MD) based model* hereafter. In both models the equilibrium structure of the molecules was estimated using force-field computations (PCFF force field in Cerius 2, Accelrys, San Diego, CA, USA). In the simple geometrical model, the spin labels are assumed to be distributed on a cone with fixed opening angle of 25° about the backbone axis of the shape-persistent phenyleneethynylene arms. Except for free rotation about the C–C bonds of the backbone, which is mimicked by the distribution on the cone, both the backbone and the nitroxide moieties were assumed to be fully rigid. Likewise, the interspin distance, namely the distance between the centers of the N–O bonds of the nitroxide labels, was assumed to be fixed at its force-field predicted values of 3.86 nm for the biradical and 3.72 nm for the triradical. The small variation in the interspin distance due to rotation of the spin labels on a cone is thus neglected in this model.

In the MD-based model, complete motional dynamics of the radical molecules was simulated for 2 ns using Cerius 2 with the PCFF force field and a Nosé–Hoover thermostat to generate a canonical ensemble. The MD trajectory was sampled by 20,000 discrete frames. We found that using the first 5000 frames (500 ps) gave a representative picture of the sampled relative conformations of the nitroxide moieties for the biradical, whereas all 20,000 frames were needed in the triradical case. For each trajectory frame the orientation of the nitroxide label molecular frames and the corresponding interspin distance were calculated from the atom positions, assuming that the x axis of the molecular frame coincides with the N–O bond and the carbon atoms bonded to the nitrogen atom of the N–O group are as close as possible to the xy plane. All further details regarding prediction of DEER response from the structure models are discussed in the Theory section. Processing of the experimental DEER data was done using the DEERAnalysis2006 package [35], and the simulations were performed by home-written Matlab programs (available from the authors on request) using subroutines from the EasySpin package [41].

3. Theory

3.1. Isolated spin pair with full geometry correlation of the two spins

Theoretical treatment of DEER relies on the concept of the dipolar coupled spin pair. The entire sample is considered as an ensemble of such spin pairs in which individual pairs act together and contribute to the total sample response. DEER experiments at conventional m.w. frequencies (X-band) provide mainly information on the pair correlation function, i.e, on the interspin distance distribution information [31,32,35]. Furthermore, information on the spin concentration and possible clustering of the probed spins can be extracted from the DEER response [10,21,35]. Intrinsically, in addition to the distance information, the DEER signal depends on the relative orientation of the molecular frames of the dipolar coupled electron spins and the orientation of the spin–spin vector with respect to these frames [37,38], as shown in Fig. 4. For simplicity we first assume an isolated pair of spins A and B. The static spin Hamiltonian in the high-field approximation is given by [11,34]

$$\hat{H}/\hbar = \Omega_A \hat{S}_z^A + \Omega_B \hat{S}_z^B + \omega_{dd} \hat{S}_z^A \hat{S}_z^B - \frac{\omega_{dd}}{2}\left(\hat{S}_x^A \hat{S}_x^B + \hat{S}_y^A \hat{S}_y^B\right) \quad (1)$$

in which Ω_A and Ω_B are the resonance offsets of the observed A and pumped B spin due to the hyperfine and g-anisotropy; and ω_{dd} is the dipole–dipole coupling. The last term on the right-hand side of Eq. (1) is the pseudosecular or flip–flop term, which can be dropped when $\omega_{dd}/2$ is much smaller than both the excitation bandwidth of the microwave pulses and the difference of the resonance frequencies of the two spins [42], as is the case for the measurements performed in this work. Neglecting this pseudosecular term, the time-domain DEER signal arising from the dipolar coupled pair of spins is given by [10]:

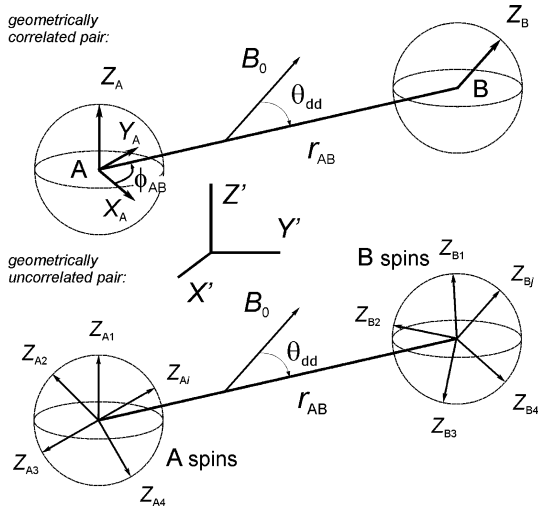

Fig. 4. Coordinate frames for a geometrically correlated spin pair (top) and a geometrically uncorrelated pair (bottom). Pair geometry is defined with respect to the molecular frame of nitroxide label A by six parameters: the interspin distance r_{AB}, the polar angles θ_{AB}, ϕ_{AB} specifying orientation of the dipolar axes in molecular frame A, and Euler angles α, β, γ defining relative orientation of the frame B with respect to the frame A. In numerical computations all frames are defined with respect to a common reference frame $X'Y'Z'$ that is chosen to reflect symmetry of the structure in the simple geometrical model or is the coordinate frame of the molecular dynamics (MD) trajectory frame in the MD-based model.

$$V(t,\theta_{dd},r) = 1 - \lambda_{AB}[1-\cos(\omega_{dd}(\theta_{dd},r_{AB})t)],$$
$$\omega_{dd}(\theta_{dd},r_{AB}) = \frac{1}{r_{AB}^3}\frac{|\mu_B|^2 g_A g_B}{\hbar}(3\cos^2\theta_{dd}-1) \quad (2)$$

where θ_{dd} is the angle between the spin–spin vector and the external magnetic field, λ_{AB} is the modulation depth, which depends on the probability to excite the B spin, μ_B is the Bohr magneton, g_A and g_B are the g-factors of the A and B spins, respectively. The modulation frequency of the DEER signal $\omega_{dd}(\theta_{dd},r_{AB})$ depends on the interspin distance r_{AB} and the angle θ_{dd} between the dipole–dipole axis and the magnetic field. Furthermore, we assume in this section a fixed relative orientation of the molecular frames of the two spins and a fixed orientation of the spin–spin vector with respect to these frames, i.e., full orientation correlation of the two spins.

For a macroscopically disordered sample, Eq. (2) has to be averaged over angle θ_{dd} with the usual weighting $\sin\theta_{dd}$. An additional weighting factor $f_A(\theta_{dd})$ arises from orientation selection of the observer spins A, since at a given excitation position a set of orientations of the molecular frame of spin A with respect to the magnetic field is selected. Since the orientation of the spin–spin vector in the molecular frame is fixed, also a set of orientations of the spin–spin vector with respect to the magnetic field is selected.

Orientation selection enters Eq. (2) in a second way due to the dependence of the modulation depth λ_{AB} on θ_{dd}. Consider all spin pairs in which the A spin was selected by observer orientation selection. Due to the fixed orientation of the molecular frame of the B spins with respect to the one of the A spins, this corresponds to a selection of orientations of the molecular frame of the B spins. However, as the pump pulse is also selective with respect to the orientation of the molecular frame of spin B, only a fraction of these preselected B spins is inverted. Generally, this fraction depends on the direction of the magnetic field with respect to the two molecular frames and thus implicitly on θ_{dd}. The weighting with factors $f_A(\theta_{dd})$ and $\lambda_{AB}(\theta_{dd})$ causes a frequency selection in the dipolar spectrum, which thus does no longer adopt the shape of a Pake pattern.

These considerations have to be somewhat extended if the relative orientations of the two molecular frames are not fixed. All possible situations fall in a range between two limiting cases: geometrically fully correlated spin pairs as discussed above and fully uncorrelated pairs. For fully uncorrelated pairs (bottom panel of Fig. 4), the dependences of f_A and λ_{AB} on θ_{dd} average and the undistorted Pake pattern is observed. In the following we consider the intermediate case where a correlation of the orientations of the two molecular frames exists, although these frames are not fixed with respect to each other.

3.2. DEER response from spin pairs with intermediate degree of geometrical correlation

For the sake of clarity, we continue our discussion with an example, considering a spin pair composed of two nitroxide radicals. The treatment for radicals or transition metal ions with different magnetic parameters is analogous. The nitroxide molecular frame is defined by choosing the X axis along the nitroxide N–O bond, the Z axis perpendicular to both the N–O bond and the vector connecting the two carbons that are bonded to the nitrogen of the N–O group, and finally, the Y axis perpendicular to X and Z. The geometry of the spin pair can be fully described by six parameters: r_{AB}—the interspin distance, which is well approximated by the distance between the midpoints of the two N–O bonds of the nitroxides; two polar angles θ_{AB}, φ_{AB} defining the orientation of the vector $\vec{r}_{AB}$ in the molecular frame of spin A; and three Euler angles α,β,γ which relate the molecular frame of spin A to the molecular frame of spin B.

To predict the sample response in DEER, numerical powder averaging over all orientations of the magnetic field B_0 on the unit sphere has to be performed. In the general case this averaging proceeds in the following way. The problem is represented in a common reference frame X′Y′Z′, in which the set of B_0 orientations is specified (Fig. 4). For every orientation the dipolar angle is calculated:

$$\theta_{dd} = \arccos\left(\frac{\vec{r}_{AB}\cdot\vec{B}_0}{r_{AB}B_0}\right) \quad (3)$$

and the corresponding dipolar frequency $\omega_{dd}(\theta_{dd}, r_{AB})$ is obtained using Eq. (2). Then the resonance frequencies of spins A and B are calculated for this field orientation.

For the geometrically fully correlated spin pair discussed above a given orientation of the spin–spin vector (angles θ_{AB}, φ_{AB}) selects a unique orientation of the molecular frame of the A spin and, consequently a single value ν_A of the resonance frequency. Likewise, there is a unique relative orientation of the B spin molecular frame defined by angles α,β,γ, and thus only one resonance frequency ν_B. When flexibility of the geometrical arrangement of a spin pair increases, the selected region in orientation space broadens. This results in a situation where more and more pairs of ν_A and ν_B correspond to the same orientation of the spin–spin vector, the pair becomes less correlated. A quantitative description can be obtained by computing $\omega_{dd}(\theta_{dd}, r_{AB})$ and the excited fractions of spins A and B (f_A and f_B, respectively) for each field orientation. In other words, the modulation depth at a given orientation $\lambda_{AB}(\theta_{dd})$ is then given by:

$$\lambda_{AB}(\theta) = f_{A,1}(\Omega_{A,1})f_{B,2}(\Omega_{B,2}) + f_{A,2}(\Omega_{A,2})f_{B,1}(\Omega_{B,2}) \tag{4}$$

Note that we have redefined λ_{AB} to include orientation selection of both observer and pumped spins, so that the powder average of Eq. (2) does no longer require an additional factor for observer spin orientation selection. Two terms in Eq. (4) appear because of the complete overlap of the EPR spectra of the two nitroxide radicals. Therefore, both spins are indistinguishable, and each of them can be excited by either frequency ν_1 or ν_2. In Eq. (4), the fraction of spins A excited by frequency ν_1 is called $f_{A,1}$, whereas that excited by frequency ν_2 is called $f_{A,2}$. An analogous notation applies for spins B. The resonance offsets in Eq. (4) are thus:

$$\begin{aligned} \Omega_{A,1} &= \nu_1 - \nu_A \\ \Omega_{B,2} &= \nu_2 - \nu_B \end{aligned} \quad \text{and} \quad \begin{aligned} \Omega_{A,2} &= \nu_2 - \nu_A \\ \Omega_{B,1} &= \nu_1 - \nu_B \end{aligned} \tag{5}$$

The excited fractions of spins A and B as functions of resonance offset Ω can be calculated from the normalized excitation profile of the observer pulse sequence $p_A(\Omega)$ and the pump pulse efficiency $p_B(\Omega)$, which in turn can be obtained as the four-pulse DEER echo intensity and as an efficiency of the coherence transfer $\hat{S}_{x,A}\hat{S}_B^{\alpha} \leftrightarrow \hat{S}_{x,A}\hat{S}_B^{\beta}$, respectively [34].

We now consider the case of a geometrically fully uncorrelated spin pair. Since there is no correlation between relative orientations of the molecular frames of spins A and B, the averaging over the orientations of the two frames (over the angles θ_{AB},φ_{AB} and α,β,γ) can be done independently. This results in complete independence of the experimental dipolar frequency on the experimental pulse positions and their excitation bandwidth as already mentioned above, because for any of those the dipolar angle will necessarily run over all its values from 0 to 90° yielding in turn the set of all values of $\omega_{dd}(\theta_{dd}, r_{AB})$ from $\omega_{dd\perp}$ to $\omega_{dd//}$. The fractions of excited spins in this case are given by:

$$f_A = \frac{\int p_A(\Omega)I(\Omega)d\Omega}{\int I(\Omega)d\Omega} \quad \text{and} \quad f_B = \frac{\int p_B(\Omega)I(\Omega)d\Omega}{\int I(\Omega)d\Omega} \tag{6}$$

in which $I(\Omega)$ is the spectral lineshape function. The time-domain DEER response for the fully uncorrelated spin pair thus has the form of Eq. (7) corresponding to a Pake pattern in frequency domain:

$$V_{pair}(t) = V_r(t,r) = V_{ID}(t)\int_0^{\pi/2} V(t,\theta,r)\sin\theta d\theta \tag{7}$$

3.3. Numerical simulation for intermediate degree of correlation

Theoretical 2D patterns that correlate the dipolar spectrum (dipolar frequency axis) to the EPR spectrum (magnetic field axis) were calculated for the model samples within the simple geometrical model and the MD-based model. In these simulations, all coordinate frames of the problem were related to a common reference frame. An array of the magnetic field orientations in this reference frame was generated using EasySpin [41] thus providing an almost uniform distribution of the B_0 orientations on the unit sphere. The smoothness of the simulated EPR absorption spectrum of the nitroxide served as an indication that a sufficient number of the magnetic field orientations was generated. Orientation averaging was done by calculating first the dipolar frequency ν_{dd} at each given B_0 orientation. For this the electron spins were assumed to reside in the midpoints of the N–O bonds of the nitroxides, and the vector connecting the midpoints served as a dipolar axis for a nitroxide spin pair. The dipolar angle θ_{dd} and the dipolar frequency $\nu_{dd}(\theta_{dd},r_{AB})$ were then calculated using Eqs. (3) and (2), and the corresponding dipolar doublet was generated.

Next the magnetic field vector was transformed into each of the nitroxide molecular frames and the respective polar angles within the molecular frames were calculated. Using standard expressions [1], the g value and ^{14}N hyperfine coupling of each nitroxide were obtained. Resonance frequencies for all three observer transitions with different magnetic quantum number m_I of the ^{14}N nucleus were then computed assuming an approximate magnetic field value $B_0 = 3.355$ T. The resonance frequencies were converted to resonance fields by assuming linear scaling of field with frequency for the difference between the computed resonance frequencies and the spectrometer frequency. This is a good approximation for a small range of g values as encountered in nitroxides. For each of the nine possible combinations of transitions of the two nitroxide radicals a weighting factor w_{AB} was computed from the two resonance frequencies ν_A and ν_B and the difference between the two microwave frequencies $\Delta\nu_{mw}$ assuming a square Gaussian decay of the excitation efficiency with the mismatch between the frequency differences:

$$w_{AB} = \exp\left(-\left(\frac{\Delta\nu_{total}}{\Delta\nu_{exc}}\right)^4\right), \quad \text{where} \quad \Delta\nu_{total} = \nu_A - \nu_B - \Delta\nu_{mw} \tag{8}$$

where v_A is the transition frequency of the observer spin at the given magnetic field orientation and the selected m_I value, v_B the transition frequency of the pump spin at the same magnetic field orientation and an independently selected second m_I value, Δv_{mw} is the experimental observer-pump frequency separation (20 MHz), and Δv_{exc} is the effective excitation bandwidth (15 MHz). Eq. (8) amounts to assuming a Gaussian excitation profile for the pump pulse and a Gaussian shape for the m.w. mode of the resonator with the same width. The finite bandwidth of the observer subsequence was considered by writing the dipolar doublet, intensity–weighted with factor w_{AB}, into three adjacent magnetic field columns of the 2D correlation pattern with intensity distribution 0.25:0.5:0.25. The pattern was written to the corresponding resonance field column of the observer spin.

So far, the simulation procedures for the biradical and the triradical as well as for the simple geometrical model and MD simulation were analogous. With respect to the generation of the nitroxide molecular frames they differ, as is discussed now in detail. In the *simple* geometrical model a fixed tilting angle of 25° was assumed between the X axis of the nitroxide molecular frame and the dipolar axes. This assumption is derived from a force-field model of the minimum-energy structure of a nitroxide moiety joined by an ester bond to a phenyleneethynylene backbone. For the biradical the dipolar axis was chosen along the Y' axis of the *reference* frame (top panel of Fig. 5). The Z axis of both nitroxide molecular frames are perpendicular to this Y' axis. Without loosing generality we can assume that the Z axis of the first nitroxide coincides with the Z' axis of the reference frame. Transformation from the reference frame to the first molecular frame thus involves a single rotation about the Z axis by an angle of 25°. Because of the rotational degree of freedom about the phenyleneethynylene backbone, transformation to the molecular frame of the second nitroxide (spin B, top panel of Fig. 5) involves a first rotation by an angle ϕ_{rot} about the Y' axis and a second rotation by 25° about the new Z axis. The angle ϕ_{rot} is uniformly distributed between 0 and 360°.

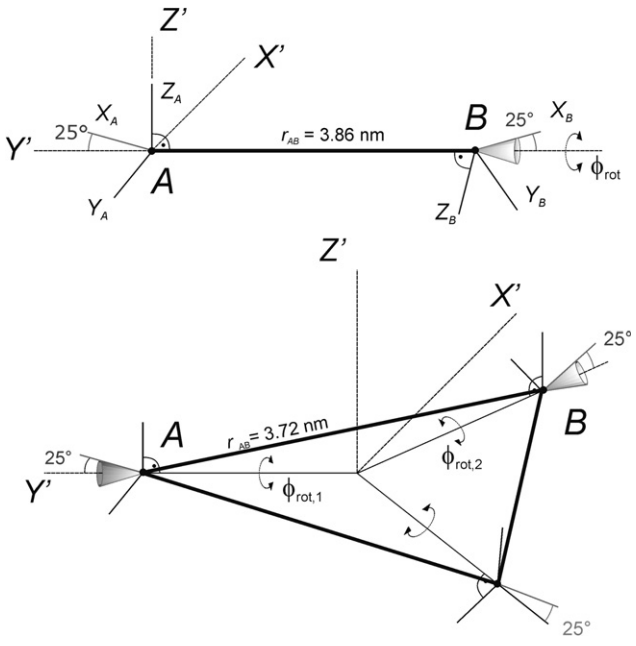

Fig. 5. Structure and dynamics of biradical (top) and triradical (bottom) molecules within the simple geometrical model.

For the triradical, the phenyleneethynylene arms were set to include 120° angles with respect to each other (bottom panel of Fig. 5). With our experimental setup the probability to excite all three spins in the same molecule simultaneously (one observer and two pumped spins) is negligible. Thus, the molecule can effectively be considered as a biradical carrying two excited spins: one observer and one pump spin. However, compared to the true biradical case, the probability that a pumped spin within the same molecule is on resonant is on average twice as high. Therefore the unmodulated fraction of the echo, which is $1 - \Delta$ for the biradical, should be only $(1 - \Delta)^2$ for the triradical, corresponding to a modulation depth $2\Delta - \Delta^2$ instead of Δ. For our experimental Δ of about 0.05, the Δ^2 term can be neglected. The triradical can thus be simulated as a biradical with twice the modulation depth. Generation of the molecular frames of the nitroxide moieties involves independent rotations by uniformly distributed angles $\phi_{rot,1}$ and $\phi_{rot,2}$ about the two phenyleneethynylene arms to which the nitroxides are attached, and an additional 120° rotation about the initial Z' axis of the reference frame, which is the C_3 symmetry axes of the tristar, for the second moiety.

In the MD based model the coordinates of the atomic positions were used to determine the molecular frames of the observer and pump spins as well as the length of the interspin vector and its orientation with respect to the external magnetic field for each of the motion frames representing the conformational dynamics of molecules of both model systems. This approach corresponds to calculating the 2D patterns for 5000 rigid spin pairs for the case of biradical and 20,000 ones—for the triradical, and summing them up to obtain the simulated pattern for the whole MD trajectory. The basic assumption behind this approach is that the conformations sampled during the MD run coincide with the conformational ensemble in a glassy frozen matrix.

4. Results and Discussions

Characteristic orientation selection effects were clearly observed already by visual inspection of the raw data. Fig. 6A shows background corrected dipolar time domain signals for the biradical taken from the X, Y and Z regions of the nitroxide g-tensor. The dipolar frequency and the modulation depth undergo variations when the observer position is changed. Note that at a dipolar evolution time t as long as 4 μs the signal-to-noise ratio is still acceptable at all orientations, as becomes clear from the dipolar spectra shown in Fig. 6B. The dipolar frequency of slightly less

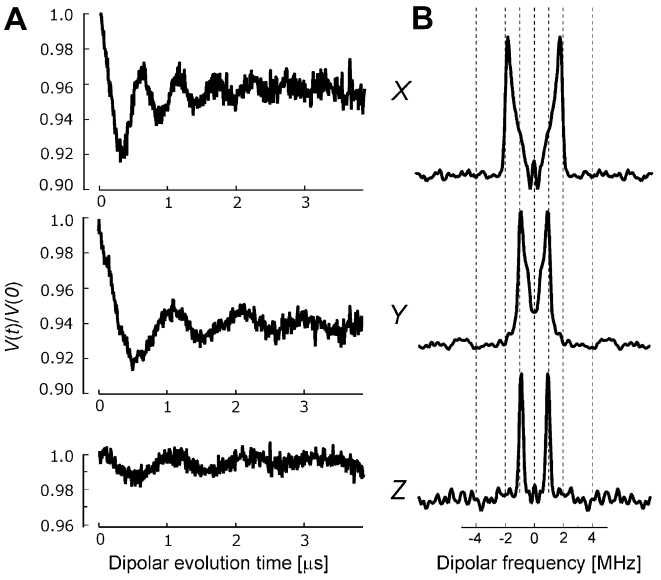

Fig. 6. High-field DEER of the biradical at canonical orientations of the *g*-tensor. Background corrected time-domain experimental traces (A) taken from *X*, *Y* and *Z* regions of the *g*-tensor orientations (sampling positions: i, iii, vi, respectively, in Fig. 3) and corresponding dipolar spectra (B).

than 2 MHz observed at the *g*-tensor orientation along *X* is close to the one expected from the simple geometrical model ($r_{AB} = 3.86$ nm, 1.81 MHz) for the dipolar axis of the radical being aligned along the magnetic field, whereas experimental ν_{dd} from the *Y* and *Z* *g*-tensor orientations are nearly equal to each other and close to 0.90 MHz. This value is expected for the perpendicular orientation of the dipolar axis with respect to the magnetic field.

A more detailed comparison of the experimental and simulated data for the biradical, including three intermediate orientations, is shown in Fig. 7. The simulated 2D patterns ν_{dd} *vs* B_0 differ between the simple geometrical model and the MD-based simulation mainly by a blurring of all features in the MD-based pattern. This is expected, as the MD simulation includes conformational degrees of freedom that are neglected in the simple model. The simulated dipolar spectra obtained by slicing the 2D patterns at the experimental observer positions generally correspond quite well with the experimental data, even for the simple geometrical model. The frequencies of the singularities of the simulated dipolar doublets are following the experimentally observed singularities throughout the full range of *g*-tensor orientations. The simulated frequencies are consistently slightly lower then the experimental ones. The reason is that the interspin distance of 3.86 nm predicted by the force field and used in the simple geometrical model simulations is an overestimate, as was already revealed by DEER at *X*-band which provided an experimental value of 3.75 nm (Fig. 8A).

The dependence of the dipolar frequency on the observer position proves that the nitroxide spin pair of the biradical is geometrically correlated to a high degree, and furthermore that the simple geometrical model already predicts the most significant features of structure and dynamics of the molecule. Indeed, since in our setup of high-field DEER experiments both observer and pump pulses select practically the same orientations of the pump and observer spins, B_0 is always nearly perpendicular to the dipolar axis if the nitroxide moieties are excited in the range between *Y* and *Z* *g*-tensor orientations (Fig. 5). Correspondently, we observe a constant frequency of the maxima of the dipolar spectrum of about 0.92 MHz in that range (data points iii, iv, v and vi on Fig. 7). Note that the shape of the dipolar spectrum at the positions iii and iv is more complicated than that at the positions v and vi, nevertheless the frequency contributions at about 0.92 MHz are dominating the lineshape. Both the simple geometrical and the MD-based model fit these shapes with almost the same quality, although it has to be said that the outer shoulders of the pattern iii are observed experimentally and in the MD-based simulation, but not in the simple geometrical model.

When changing the DEER excitation positions from *Y* towards *X* orientations of the nitroxide *g*-tensor, the experimental dipolar spectrum undergoes gradual transformations. The lines broaden and the lineshape becomes complex, and finally the maximum value of the dipolar frequency of about 1.83 MHz is observed at the position i, being one of the *X* *g*-tensor orientations. This value is in accordance with the simple model prediction of 1.81 MHz, as well as it agrees reasonably well with the $\nu_{\|}$ value of 1.97 MHz for an interspin distance of 3.75 nm (*X*-band experimental value). The shape of the dipolar spectrum is still complex in the *X* region, in addition to the $\nu_{\|}$ feature, substantially lower frequencies are present. This is explained by the structure of the biradical molecule: a fixed angle of about 25° between the nitroxide N–O bond and the backbone lowers the probability to excite orientations of the dipolar axis that are strictly parallel to the field and introduces other orientations.

When comparing the experimental dipolar lineshapes with simulations, one has to keep in mind that uncertainties in background correction can lead to intensity artifacts close to zero frequency. We estimate that the experimental lineshapes are therefore unreliable between −0.3 and 0.3 MHz. Considering this, the spectra simulated within the *MD-based model* (green lines in Fig. 7C) represent the experimental lineshape (black lines) significantly better than the spectra simulated with the simple geometrical model (red lines). Furthermore, the shape and the width of the model interspin distance distribution reasonably reproduce the experimental shape and width except for the above-mentioned shift of the distribution maximum towards longer distances (Fig. 8A). The remaining differences are probably due to an underestimate of the flexibility of the phenyleneethynylene backbone by the force-field parameters. The shape of the distance distribution depends on this backbone flexibility, with the sharp maximum corresponding to the largest possible distance encountered for a fully stretched backbone, and a more gradual decrease

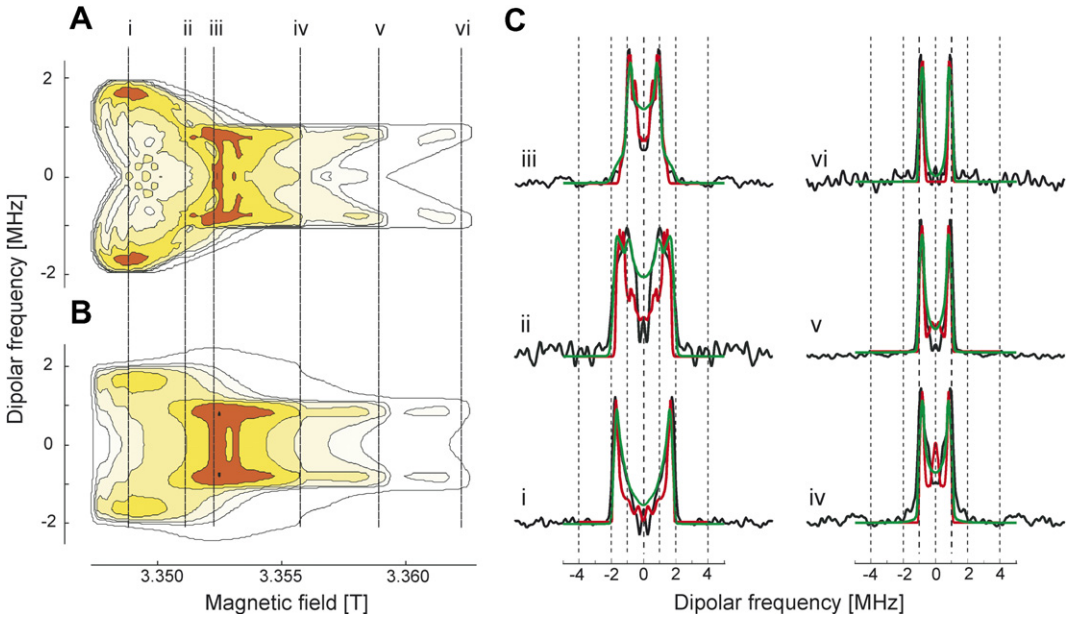

Fig. 7. Model simulations of 2D correlation patterns of the dipolar frequency ν_{dd} vs the magnetic field B_0 for the biradical and comparison with experiment. (A) 2D pattern obtained within the simple geometrical model. (B) 2D pattern obtained within the MD-based model. (C) Comparison of slices of the 2D patterns at the experimental sampling positions defined in Fig. 3 (red lines: simple geometrical model, green lines: MD-based model) with the experimental data (black lines).

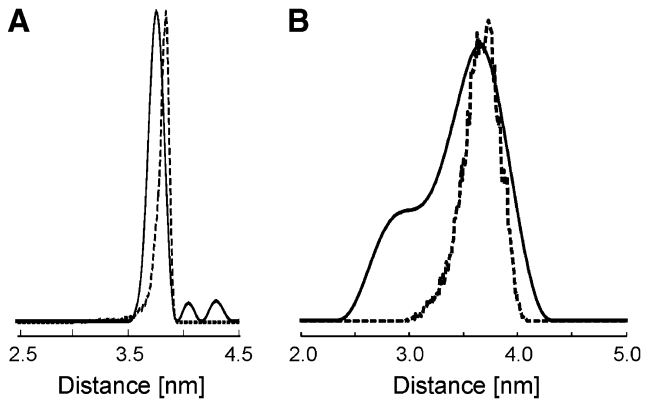

Fig. 8. Interspin distance distributions predicted by the MD-based model (dashed lines) and obtained experimentally at *X*-band frequencies (solid lines) for the biradical (A) and the triradical (B).

towards shorter distances. The fully stretched conformation has the lowest energy and therefore the highest probability. With increasing backbone bending the internal energy of the molecule increases and the end-to-end distance decreases. Boltzmann statistics results in a decreasing probability with increasing bending and thus with decreasing distance.

Both the simple geometrical and the MD-based model reproduce quite well the experimental modulation depth in the *Y*–*Z* region of the *g*-tensor orientations (Fig. 9A). The reason of the decrease of λ_{AB} when going from *Y* to *Z* is a decrease in the total number of excited spins. Experimental modulation depths λ_{AB} in the *X*–*Y* region are reproduced reasonably well by the MD-based model, whereas the simple geometrical model fails in that spectral region.

Regarding the triradical, our two-spin simulations for the limit of low modulation depth reproduce the trend in the experimental results quite well throughout the entire sampled range of the *g*-tensor orientations (Fig. 10). However, the lineshapes are not as well reproduced as for the biradical case. Furthermore, the simulated distance distribution predicted by the MD-based model deviates from the experimental one observed by DEER at *X*-band (Fig. 8B). Again this may be a result of force-field parameters that underestimate backbone flexibility. For the particular geometry of the triradical, this flexibility is expected to lead to stronger changes in the distance distribution than for the linear biradical, as the nitroxide moieties in the triradical can move much more strongly towards each other. This effect introduces contributions at shorter distances that are apparent in the experimental result in Fig. 8B but are not reproduced by the simulation. Furthermore, experimental dipolar frequencies are generally somewhat smaller than predicted by both models. Finally, both the simple geometrical model and the MD-based model reproduce quite well the dependence of modulation depth on field in the *Y*–*Z* region of the orientations, but both of them fail in the *X*–*Y* region (Fig. 9B). High-field DEER thus appears to reveal to which extent a molecular modeling approach reproduces the true conformational distribution of a macromolecule. Hence, such measurements could aid development of more sophisticated modeling approaches.

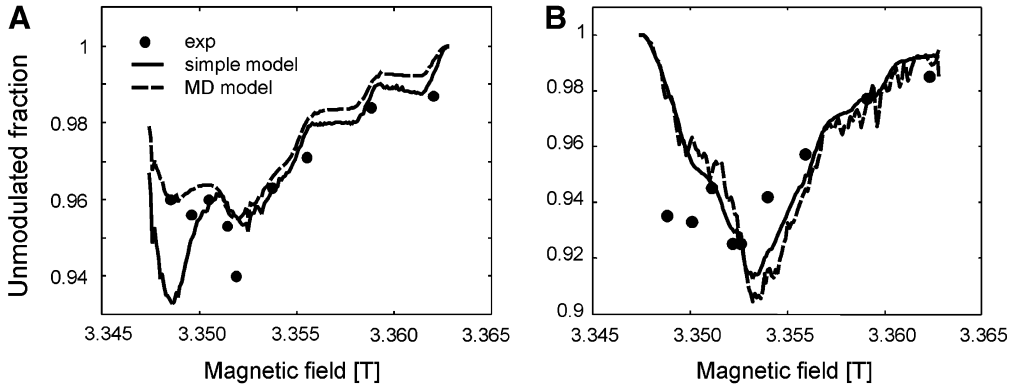

Fig. 9. Dependence of the modulation depth on the observer field in high-field DEER for the biradical (A) and triradical (B). Full circles are experimental data, solid lines predictions by the simple geometrical model, and dashed lines predictions by the MD-based model.

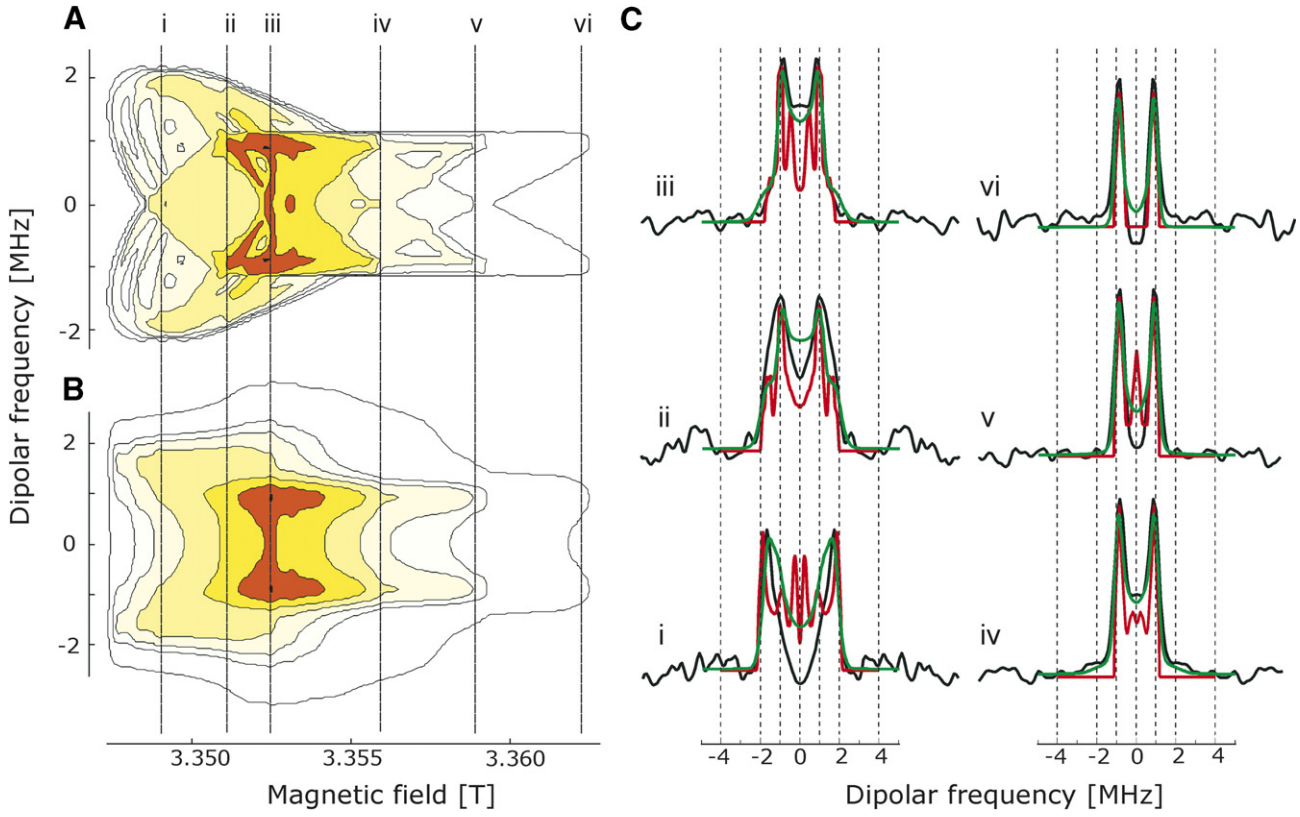

Fig. 10. Model simulations of 2D correlation patterns of the dipolar frequency ν_{dd} vs the magnetic field B_0 for the triradical and comparison with experiment. (A) 2D pattern obtained within the simple geometrical model. (B) 2D pattern obtained within the MD-based model. (C) Comparison of slices of the 2D patterns at the experimental sampling positions defined in Fig. 3 (red lines: simple geometrical model, green lines: MD-based model) with the experimental data (black lines).

5. Conclusions

Orientation selection in high-field DEER causes characteristic magnetic field dependencies of the dipolar frequencies and the modulation depth for compounds with limited but significant structural flexibility, namely a shape-persistent biradical and a shape-persistent triradical with conformationally flexible spin labels. Experimental dipolar data that were obtained for the first time with a commercial power-upgraded *W*-band spectrometer are in a good accord with simulations based on two structural models with different degree of sophistication—a model based on simple geometrical considerations and a model based on a molecular dynamics simulation. From a technical point of view, it was found that orientation-selective DEER experiments at *W*-band frequencies can be performed with a critically coupled cylindrical cavity despite its narrow bandwidth, as the apparent bandwidth problem can be overcome by applying experimental methodology in which the positions of the pump and the observer pulses of the

DEER sequence are placed at a fixed small frequency difference of about 20 MHz and the orientation selection depends only on changes in the magnetic field. Such experiments can reveal whether molecular modeling approaches provide correct conformational ensembles for macromolecules. This question is of particular interest for elucidating conformational distributions of the labels in spin-labeled biomacromolecules and thus for improving the precision and reliability of distance measurements between backbone atoms in these molecules with spin-label EPR techniques. Work along these lines is now in progress.

Acknowledgments

The authors thank Herbert Zimmermann for a generous gift of perdeuterated *o*-terphenyl and SFB 625 of Deutsche Forschungsgemeinschaft for financial support.

References

[1] A. Schweiger, G. Jeschke, Principles of Pulse Electron Paramagnetic Resonance, Oxford University Press, Oxford, 2001.
[2] W. Hubbell, C. Altenbach, Investigation of structure and dynamics in membrane proteins using site-directed spin labeling, Curr. Opin. Struct. Biol. 4 (1994) 566–573.
[3] W. Hubbell, A. Gross, R. Langen, M. Lietzow, Recent advances in site-directed spin labeling of proteins, Curr. Opin. Struct. Biol. 8 (1998) 649–656.
[4] W. Hubbell, D. Cafiso, C. Altenbach, Identifying conformational changes with site-directed spin labeling, Nat. Struct. Biol. 7 (2000) 735–739.
[5] K. Möbius, A. Savitsky, C. Wegner, M. Plato, M. Fuchs, A. Schnegg, A. Dubinsky, Y. Grishin, I. Grigor'ev, M. Künn, D. Duché, H. Zimmermann, H. Steinhoff, Combining high-field EPR with site-directed spin labeling reveals unique information on proteins in action, Magn. Reson. Chem. 43 (2005) S4–S16.
[6] J. Pyka, J. Ilnicki, C. Altenbach, W. Hubbell, W. Froncisz, Accessibility and dynamics of nitroxide side chains in T4 lysozyme measured by saturation recovery EPR, Biophys. J. 89 (2005) 2059–2068;.
[7] A. Shvetsov, J. Stamm, M. Phillips, D. Warshaviak, C. Altenbach, P. Rubenstein, K. Hideg, W. Hubbell, E. Reisler, Conformational dynamics of loop 262-274 in G- and F-actin, Biochemistry 45 (2006) 6541–6549.
[8] H.-J. Steinhoff, Methods for study of protein dynamics and protein-protein interaction in protein-ubiquitination by electron paramagnetic resonance spectroscopy, Front. Biosci. 7 (2002) C97–C110.
[9] A. Milov, K. Salikhov, M. Shirov, Application of ELDOR in electron spin echo for paramagnetic center space distributions in solids, Fiz. Tverd. Tela (Leningrad) 23 (1981) 957–982.
[10] A. Milov, A. Ponomarev, Yu. Tsvetkov, Electron–electron double-resonance in electron spin echo: model biradical systems and the sensitized photolysis of decalin, Chem. Phys. Lett. 110 (1984) 67–72.
[11] M. Pannier, S. Veit, A. Godt, G. Jeschke, H.W. Spiess, Dead-time free measurement of dipole-dipole interactions between electron spins, J. Magn. Reson. 142 (2000) 331–340.
[12] S. Saxena, J. Freed, Double quantum two-dimensional Fourier transform electron spin resonance: distance measurements, Chem. Phys. Lett. 251 (1996) 102–110.
[13] P. Borbat, J. Freed, Multiple-quantum ESR and distance measurements, Chem. Phys. Lett. 313 (1999) 145–154.
[14] P. Borbat, H. Mchaourab, J. Freed, Protein structure determination using long-distance constraints from double-quantum coherence ESR: study of T4 lysozyme, J. Am. Chem. Soc. 124 (2002) 5304–5314.
[15] M. Persson, J. Harbridge, P. Hammarstrom, R. Mitri, L.-G. Martensson, U. Carlsson, G. Eaton, S. Eaton, Comparison of electron paramagnetic resonance methods to determine distances between spin-labels on human carbonic anhydrase II, Biophys. J. 80 (2001) 2886–2897.
[16] C. Elsässer, M. Brecht, R. Bittl, Pulsed electron–electron double resonance on multinuclear metal clusters: assignment of spin projection factors on the dipolar interaction, J. Am. Chem. Soc. 124 (2002) 12606–12611.
[17] Z. Zhou, S.C. DeSensi, R.A. Stein, S. Brandon, M. Dixit, E.J. McArdle, E.M. Warren, H.K. Kroh, L. Song, C.E. Cobb, E.J. Hustedt, A.H. Beth, Solution structure of the cytoplasmic domain of erythrocyte membrane band 3 determined by site-directed spin labeling, Biochemistry 44 (2005) 15115–15128.
[18] J. Banham, C. Timmel, R. Abbott, S. Lea, G. Jeschke, The characterization of weak protein-protein interactions: evidence from DEER for the trimerization of a von Willebrand Factor A domain in solution, Angew. Chem. Int. Edit. 118 (2006) 1058–1061.
[19] G. Jeschke, C. Wegener, M. Nietschke, H. Jung, H.-J. Steinhoff, Interresidual distance determination by four-pulse double electron–electron resonance in an integral memrane protein: the Na^+/proline transporter PutP of Escherichia coli, Biophys. J. 86 (2004) 2551–2557.
[20] G. Jeschke, A. Bender, T. Schweikardt, G. Panek, H. Decker, H. Paulsen, Localization of the N-terminal domain in light-harvesting chlorophyll a/b protein by EPR measurements, J. Biol. Chem. 280 (2005) 18623–18630.
[21] D. Hilger, H. Jung, E. Padan, C. Wegener, K.-P. Vogel, H.-J. Steinhoff, G. Jeschke, Assessing oligomerization of membrane proteins by four-pulse DEER: pH-dependent dimerization of NhaA Na^+/H^+ antiporter of E. coli, Biophys. J. 89 (2005) 1328–1338.
[22] I. Borovykh, S. Ceola, P. Gajula, P. Gast, H.-J. Steinhoff, M. Huber, Distance between a native cofactor and a spin label in the reaction centre of Rhodobacter sphaeroides by a two-frequency pulsed electron paramagnetic resonance method and molecular dynamics simulations, J. Magn. Reson. 180 (2006) 178–185.
[23] O. Schiemann, N. Piton, Y. Mu, G. Stock, J. Engels, T. Prisner, A PELDOR-based nanometer distance ruler for oligonucleotides, J. Am. Chem. Soc. 126 (2004) 5722–5729.
[24] A. Milov, Y. Tsvetkov, F. Formaggio, M. Crisma, C. Toniolo, J. Raap, Self-assembling properties of membrane-peptides studied by Peldor and cw-ESR spectroscopies, J. Am. Chem. Soc. 122 (2000) 3843–3848.
[25] M. Pannier, V. Schädler, M. Schöps, U. Wiesner, G. Jeschke, H.-W. Spiess, Determination of ion cluster size and cluster-to-cluster distances in ionomers by four-pulse double electron–electron resonance spectroscopy, Macromolecules 33 (2000) 7812–7818.
[26] G. Jeschke, Determination of the nanostructure of polymer materials by electron paramagnetic resonance spectroscopy, Macromol. Rapid Comm. 23 (2002) 227–246.
[27] G. Jeschke, A. Godt, Co-conformational distribution of nanosized [2]catenanes determined by pulse EPR measurements, Chem. Phys. Chem 4 (2003) 1328–1334.
[28] D. Hinderberger, O. Schmelz, M. Rehahn, G. Jeschke, Electrostatic site attachment of divalent counterions to rodlike ruthenium(II) coordination polymers characterized by EPR, Angew. Chem. Int. Edit. 43 (2004) 4616–4621.
[29] A. Milov, A. Maryasov, Y. Tsvetkov, Pulsed electron double resonance (PELDOR) and its applications in free-radicals research, Appl. Magn. Reson. 15 (1998) 107–143.
[30] A. Milov, B. Naumov, Yu. Tsvetkov, The effect of microwave pulse duration on the distance distribution function between spin labels obtained by PELDOR data analysis, Appl. Magn. Reson. 26 (2004) 587–599.
[31] G. Jeschke, Distance measurements in the nanometer range by pulse EPR, Chem. Phys. Chem 3 (2002) 927–932.
[32] G. Jeschke, Data analysis procedures for pulse ELDOR measurements of broad distance distributions, Appl. Magn. Reson. 26 (2004) 223–224.

[33] G. Jeschke, A.BenderH. Paulsen, H. Zimmermann, A. Godt, Sensitivity enhancement in pulse EPR distance measurements, J. Magn. Reson. 169 (2004) 1–12.
[34] G. Jeschke, H. Zimmermann, A. Godt, Isotope selection in distance measurements between nitroxides, J. Magn. Reson. 180 (2006) 137–146.
[35] G. Jeschke, V. Chechik, P. Ionita, A. Godt, H. Zimmermann, J. Banham, C.R. Timmel, D. Hilger, H. Jung, DeerAnalysis2006—a comprehensive software package for analyzing pulsed ELDOR data, Appl. Magn. Reson. (in press).
[36] Y.-W. Chiang, P. Borbat, J. Freed, The determination of pair distance distributions by pulsed ESR using Tikhonov regularization, J. Magn. Reson. 172 (2005) 279–295.
[37] R. Larsen, D. Singel, Double electron–electron resonance spin-echo modulation: spectroscopic measurement of electron spin-pair separations in orientationally disordered solids, J. Chem. Phys. 98 (1993) 5134–5146.
[38] A. Maryasov, Y.TsvetkovJ. Raap, Weakly coupled radical pairs in solids: ELDOR in ESE structure studies, Appl. Magn. Reson. 14 (1998) 101–113.
[39] V. Denysenkov, T. Prisner, J. Stubbe, M. Benatti, High-frequency 180 GHz PELDOR, Appl. Magn. Reson. 29 (2005) 375–384.
[40] A. Godt, C. Franzen, S. Veit, V. Enkelmann, M. Pannier, G. Jeschke, EPR probes with well-defined, long distances between two or three unpaired electrons, J. Org. Chem. 65 (2000) 7575–7582.
[41] S. Stoll, A. Schweiger, EasySpin, a comprehensive software package for spectral simulation and analysis in EPR, J. Magn. Reson. 178 (2006) 42–55.
[42] G. Jeschke, H.W. Spiess, Distance Measurements in Solid-State NMR and EPR Spectroscopy, Lect. Notes Phys. 684 (2006) 21–63.